Digest Journal of Nanomaterials and Biostructures Vol. 19, No. 1, January - March 2024, p. 229 – 241

Composition dependent structural, electrical, and optical properties of p-type InSb thin film for homojunction device application

K. Shriram[a,*], R. R. Awasthi[b], B. Das[a]
[a] *Department of Physics, University of Lucknow, Lucknow-226007, U.P., India*
[b] *Faculty of Engineering and Technology, Khwaja Moinuddin Chisti Language University, Lucknow- 226013, U.P., India*

A key component of IR detectors and sources is the indium antimonide, having a narrow direct band gap of 0.17eV. The present paper deals with the fabrication, structural, electrical, and optical properties of p-type indium antimonide thin films of about 300 nm thickness by thermal evaporation technique on ultrasonically cleaned glass substrates with different compositions having formula In_xSb_{1-x}. Hall measurement indicates that the as-fabricated films were p-type, having a carrier concentration of 0.435 x$10^{18}$to 1.590 x10^{18} cm^{-3} and mobility of 3.29 – 6.62 cm^2/V-s for the film thickness of 300 nm. The activation energy (E_a) was determined and found to be in the range of 0.710 – 0.518 eV from the measurement of electrical resistivity of thin films in the temperature ranges of 313 K - 363 K. X-ray diffraction studies revealed the diffraction peaks (111), (220), and (311) confirm the bulk and thin film formation of InSb polycrystalline materials. The grain size (D), dislocation density(δ), and Strain (ε) have been calculated using XRD data. The lattice parameter (a=b=c) was found to be 6.7074Å from the X-ray diffraction method (XRD). The surface morphology study of thin film through scanning electron microscope reveals the formation of nano-grains with grain size ranging between 7.63 nm to 26.32 nm and surface area of 672-1343 nm^2.

(Received September 23, 2023; Accepted January 31, 2024)

Keywords: Thin film, PXRD, I-V characteristics, Band gap

1. Introduction

Materials for modern electronic devices must, from a practical perspective, fulfill a number of fundamental characteristics, including good material quality, scalability, high electronic performance, repeatability, and a low-cost synthesis process[1]. Due to their extraordinary electronic characteristics, III-V semiconducting thin films find extensive use in cutting-edge opto- and nanoelectronics systems[1]. A promising material among the III-V group binary compounds is the semiconducting Indium Antimonide (InSb). These compounds have a zincblende structure, with an In-Sb nearest neighbor distance of 2.80 Å. The compound melting point is 523 °C. The remarkable characteristics of compound (InSb) are that it is suitable as an infrared detector and filter due to its smallest bandgap (0.17 eV) at 300 K among all III-V binaries, which corresponds to IR wavelength (6.2 μm)[2]. During the last decade, several samples of Indium Antimonide (bulk and thin films) have been prepared by different techniques and subjected to Hall measurements (electrical resistivity, carrier concentration, and mobility). Also, various research reports on the thin-film deposition of indium antimonide lead to the fabrication of interesting devices such as Hall sensors and magneto resistors [3], speed-sensitive sensors[4], and magnetic sensors[5].Furthermore, 1-D Indium Antimonide nanowires have a Bohr exciton radius of 60 nm, making them a desirable semiconductor for quantum effect studies [6], [7]. The presence of cation vacancies in Antimony-rich Indium Antimonide exhibits p-type conduction, whereas the anion vacancies in Indium-enriched Indium Antimonide, exhibit n-type conduction. Since the current study's objective is to develop p-type indium antimonide thin films, antimony-enriched non-stoichiometric InSb powder with various indium and antimony compositions was created. This is a

[*] Corresponding author: kartikeyshriram@gmail.com
https://doi.org/10.15251/DJNB.2024.191.229

unique method for fabricating thin films with a controlled proportion of non-stoichiometry. We used controlled non-stoichiometric starting materials to fabricate p-type InSb thin films using the thermal evaporation method. Because materials turn into a vapor state during a deposition without transitioning into a liquid state, the thermal evaporation method is more appropriate than other physical evaporation. For semiconducting device fabrication like a diode, photodiode, transistor, and photodetectors we need a junction between p-type and n-type. For optoelectronics devices, it's very important for a junction to have fewer defects and lattice mismatches. The defects create a trap state between bands, the trap state responsible for the nonradiative transition in the optoelectronic device we are interested in radiative transition. One of the key issues comes into the picture that is a lattice mismatch. In the present work, we study about lattice mismatch and critical thickness, using p-type InSb as substrate and compare with other papers that fabricate n-type InSb thin film.

2. Experimental Detail

Although various methods, including vacuum evaporation [8], metal-organic chemical vapor deposition [9], molecular beam epitaxial[10], and electron beam evaporation[11]have been reported for the fabrication of nonstoichiometry InSb thin films of both n- and p-type conduction. However, the p-type indium antimonide $In_{1-x}Sb_x$ thin films for different values of x from 0.60, 0.65, and 0.70, have been prepared via two-stage processes in the present paper. In the first stage, high-purity Indium (99.999 %) and Antimony (99.999 %) metal powder, procured from Alpha Aesar Limited (USA) were mixed and ground thoroughly in various compositions with a mortal and pastel, and then calcined for 10 hours at a vacuum of $2x10^{-5}$ torr using a molybdenum boat, and finally cooled to room temperature. This process was repeated 5 times by increasing the temperature to 10 ^{0}C in each step. In the second stage, the bulk InSb compound synthesized in the first stage was thermally evaporated on the glass slides with dimensions of (75 mm x 25 mm x 1 mm) in a closed chamber of pressure of 10^{-6} torr, with a liquid nitrogen trap. The glass slides were cleaned using chromic acid, rinsed with double-distilled water in an ultrasonic cleaner, and finally dried at 150 °C in an oven. The separation between the source material and the substrate was maintained at 120 mm. The physical parameter such as deposition rate (5-10) nm/sec were controlled using regulating electrical current flow through the boat. The deposition rate was evaluated using a quartz crystal sensor (6MHz) positioned close to the substrate. The film thickness monitor was also used to measure the film's thickness during the deposition process. The flowchart for the preparation of thin films is presented in Figure 1. After the successful fabrication of thin films of 300 nm thickness, the phase identification and crystallinity of the prepared thin films were studied using the Panalytical X'Pert Pro X-ray diffractometer with CuK_α Radiation (λ = 1.5406 Å). The Grazing angle x-ray diffraction (GAXRD) measurements were carried out by fixing the glancing angle at 1° with a scanning range of 2θ from 20° to 60°. The surface morphology and chemical composition of thin films were explored through a scanning electron microscope (Carl Zeiss Gemini SEM-300) attached with energy dispersive analysis of x-ray (EDAX) detector. For the optical characterization of the synthesized thin films, UV–Visible spectrophotometer (V-670 UV-VIS-NIR) was used to record the UV-visible absorption spectra.

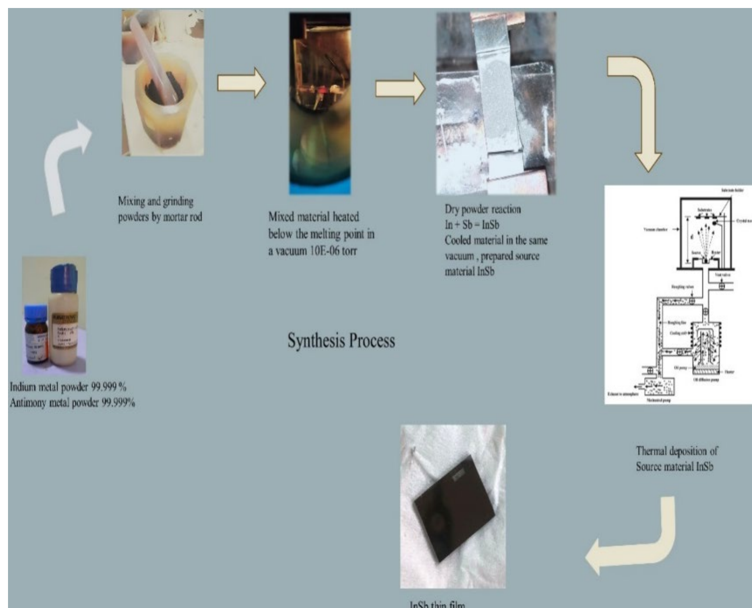

Fig. 1. Flowchart for the whole synthesis Process.

3. Result and discussion

3.1. XRD (X-Ray Diffraction Analysis)

The representative powder x-ray diffraction (PXRD) patterns of InSb source materials of different stoichiometry, prepared by solid state reaction method are shown in Figure 1. The observed x-ray diffractogram of InSb source material matches well with JCPDS (06-0208) and hence confirms the formation of the Zine blend cubic crystal structure of Indium Antimonide.

Using the full width at half maxima (FWHM) β of the peak and Debye Scherrer's formula, which is shown in equation 1, the grain size (D) for the thermally evaporated InSb thin film is calculated[12].

$$D = \frac{0.94\lambda}{\beta \cos\theta} \quad (1)$$

where λ is the X-ray wavelength used and θ is the diffraction angle, β is the width of the peak at the half maximum peak intensity. The crystal size of the sample increases with increasing Sb concentration tabulated in Table 1.

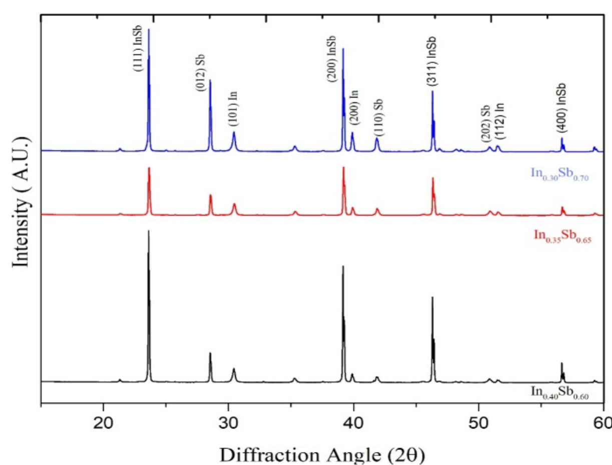

Fig. 2. X-ray diffraction patterns of InSb source material with different composition.

Table 1. Structural parameter of source material.

Composition Starting materials			
	Grain Size(nm)	Lattice parameter (nm)	Dis. Density X 10^{-5}(nm^2)
$In_{0.40}Sb_{0.60}$	104.4966	6.4908	9.157
$In_{0.35}Sb_{0.65}$	125.4321	6.4866	6.355
$In_{0.30}Sb_{0.70}$	209.2191	6.4846	2.284

3.2. Dislocation density

A crystal defect known as dislocation occurs when the lattice in one part of the crystal is misregistered in connection to another part. Dislocation is not an imperfection in equilibrium like vacancies and interstitial atoms. The growth mechanisms that include dislocation are indeed a significant issue. The Williamson and Smallman relation determines the thin film dislocation densities[13]. The dislocation density of the thin films decreases with increasing Sb concentrations it may be due to the increment of the grains size.

$$\delta = \frac{n}{D^2} \tag{2}$$

where D is the grain size and n is the constant factor equal to unity, resulting in the minimum dislocation density.

3.3. Strain

The dislocation network in the thin film is exhibited by strain. The strain in the thin film can be calculated from the relation.[14]

$$\beta = \frac{\lambda}{D\cos\theta} - \varepsilon\tan\theta. \tag{3}$$

where θ is Bragg's diffraction angle, β is the full width at half of the maximum peak intensity and $\varepsilon$is the lattice stain. It is found that lattice strains decrease with increasing the Sb concentration may be due to increases in the crystallite size of the sample tabulated in Table 2.

3.4. Lattice constant

The constant space between unit cells in a crystal lattice is known as the lattice constant or lattice parameter. Using equation (4) the lattice parameter of source material and thin films are tabulated in Tables 1 and 2 respectively. The lattice parameter of bulk and thin film material decreases with an increment of Sb concentration in composition. It may decrease due to an increment the in size of grains. Three lattice constants, indicated by the letters a, b, and c, are frequently used in three-dimensional lattices. Using Bragg's relation, the inter-planar spacing d_{hkl} for the plane (hkl)was derived from the XRD profile.[14]

$$d_{hkl} = \frac{n\lambda}{2\sin\theta} \tag{4}$$

The lattice parameter 'a' can be determined from the equation presented below for the cubic geometry.

$$\frac{1}{d^2} = \frac{(h^2+k^2+l^2)}{a^2} \quad (5)$$

3.5. Structural Parameters of thin films

In the present study, we successfully fabricate a p-type InSb thin film with lattice parameters 6.7074 Å. R K Mangal and Y K Vijay report lattice parameter 6.4840 Å[2].N K Udayshankar and H L Bhat report the lattice parameter of InSb 6.23Å with n-type semiconductivity[5]. S R Vishwakarma and Rahul report the lattice parameter of InSb thin film 6.4740 with n-type of semiconductivity[15]

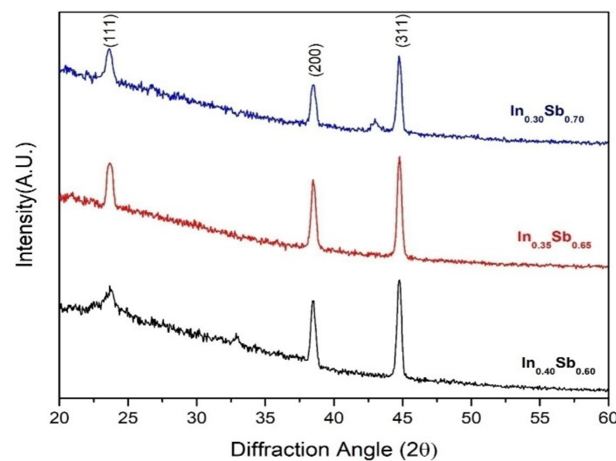

Fig. 3. GIXRD patterns of InSb thin film with different compositions.

Table 2. Structural parameter of InSb thin film.

Composition Starting materials	Composition Thin film	(311) Plane			
	EDAX	Grain Size (nm)	Dis. Density X 10^{-3} (nm^2)	Lattice parameter (nm)	Strain(ε) X 10^{-3} $Line^{-2}m^{-4}$
$In_{.40}Sb_{.60}$	40.17:59.87	24.54	1.660546	6.70948	2.04
$In_{.35}Sb_{.65}$	36.32:63.68	28.97	1.191525	6.70855	1.70
$In_{.30}Sb_{.70}$	31.36:68.64	39.76	0.632568	6.70740	1.01

3.6. Field Emission Scanning Electron Microscopy (FE-SEM) Analysis

The surface morphology of thin films is investigated using a field emission scanning electron microscope (FE-SEM) shown in the figure. It is one of the most used methods for obtaining thin film microstructure and surface morphology. The surface analysis using scanning electron microscopy can provide information about the grain size and orientation[1]

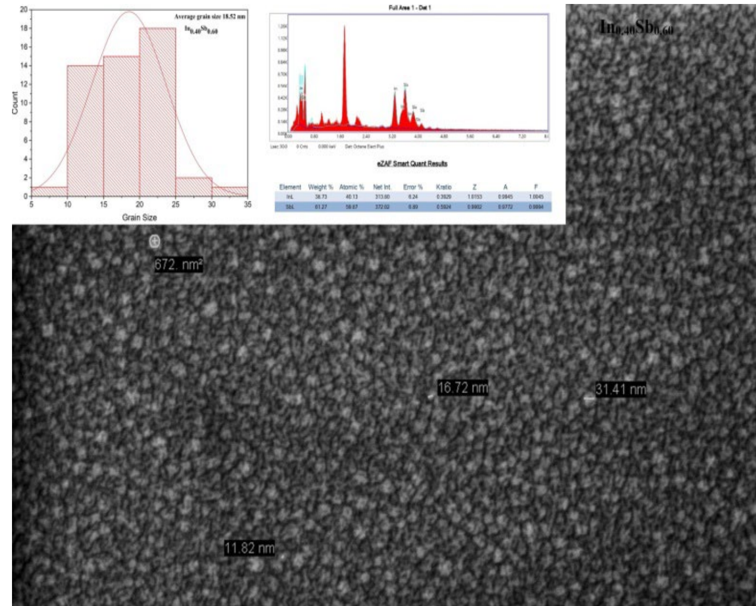

Fig. 4. FESEM of InSb (40:60).

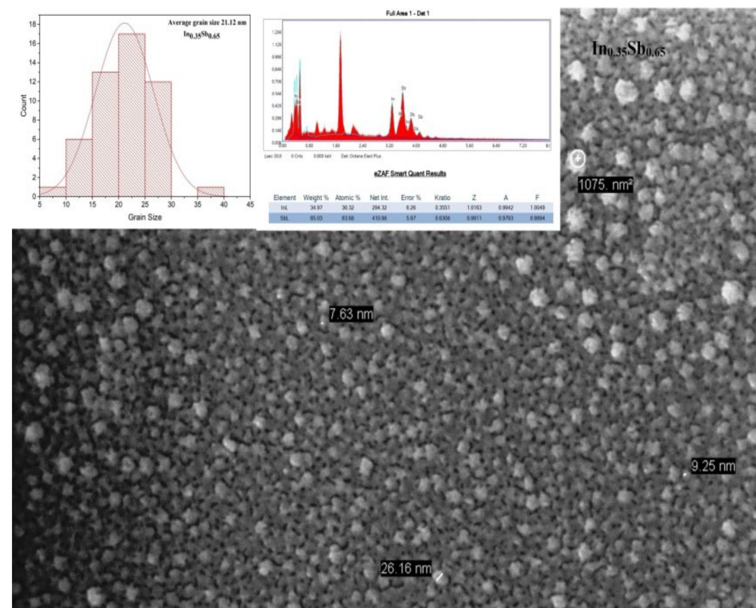

Fig. 5. FESEM of InSb (35:65).

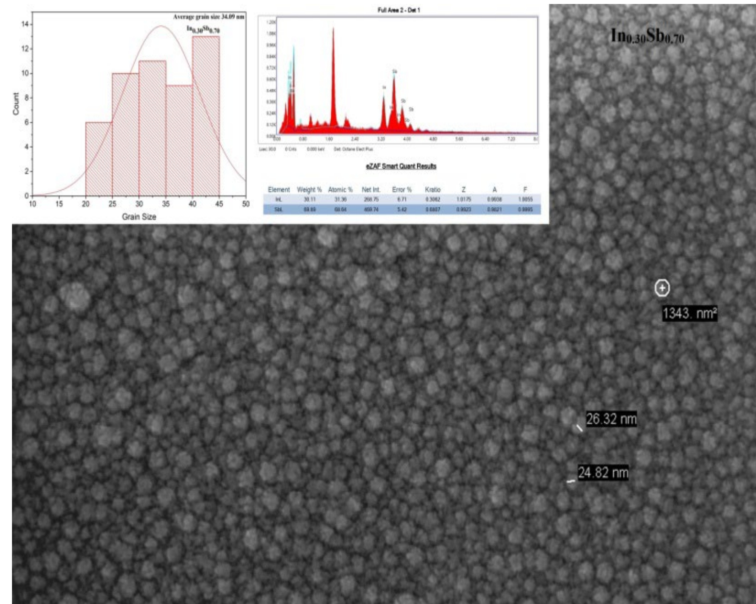

Fig. 6. FESEM of InSb (30:70).

The surface morphology of P-type InSb thin films has been examined using scanning electron micrographs (FESEM). P-type InSb films on a glass substrate are seen in SEM images in Figs. 4, 5, and 6. The deposited n-InSb films are homogeneous, without cracks or holes, well coated to the glass substrate, and the size of the crystallites is on the order of nanometers, which is validated by X-ray differentiation measurement. Scanning electron microscopy patterns also support the relationship between the size variation of crystallites and the composition ratio in source materials. In Fig.4,5, and 6, $In_{0.40}Sb_{0.60}$, $In_{0.35}Sb_{0.65}$, $In_{0.30}Sb_{0.70}$ In the formation of nanograins with an average grain of size 18.51 nm,21.12 nm, and 36.09 respectively. The chemical compositional analysis data of InSb thin films are presented in Table 2. Table 2 shows that the composition of indium and antimony in starting materials and thin films is approximately equal, with a little deviation.

3.7. Electrical properties

3.7.1. I-V Characteristics of thin films

The I-V (current-voltage) characteristic of a compound semiconductor thin film is an important aspect of its behavior and performance. The I-V characteristics of the sample show a slop straight line which revealed uniform resistivity throughout the sample. The grain growths of the film are homogenous and uniform which shows the high quality of the film[16].In fig., the I-V curve of InSb thin films shows that resistance decreases with an increase of antimony in composition it may be due to the decrement of the grains growth of thin films.

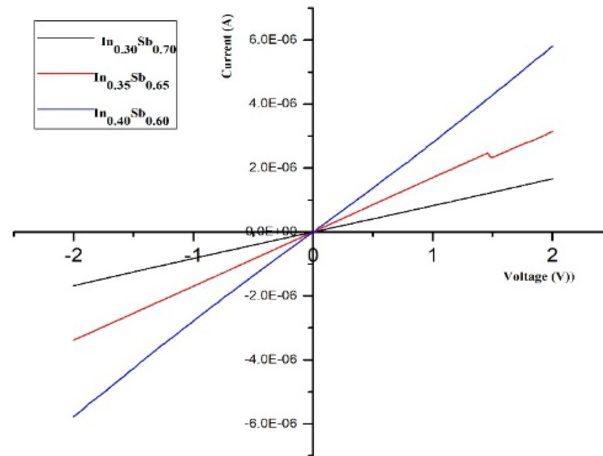

Fig. 7. I-V curve of InSb thin films for different compositions InSb thin film.

3.7.2. Four Probe for Resistivity and Activation Energy Measurement

Four Probe is a widely used method for measuring the resistivity and activation energy of the semiconductor. A collinear four-probe arrangement is made to the sample surface through the configuration of the probes in which two probes are utilized as a source of current and the other two are probes used to measure the voltage. Using four probes has the benefit of preventing inaccuracy caused by probe resistance and dividing resistance evenly between each metal probe and the substance. By applying a constant current (I) through the outer pair of probes and measuring the output voltage (V) drop between the inner pair of probes, which are separated apart by a distance of S=2 mm, a four-probe setup is used to calculate the electrical resistivity (ρ).

$$\rho = \frac{V \times 2S}{I \times G_7\left(\frac{w}{S}\right)} \tag{6}$$

where $G_7\left(\frac{w}{S}\right) = \frac{2S}{w \log 2}$ is the correction factor, w is the thickness of the thin film, and ρ is the resistivity of sample.

3.8. Activation Energy

The following equation was used to calculate the activation energy of the charge carrier using the temperature-dependent electrical conductivity of P-type InSb thin films.[17]

$$\sigma_t = \sigma_o exp\left(\frac{-\Delta E_a}{KT}\right) \tag{7}$$

where $\Delta E_a$is the activation energy, K and $\sigma_o$is the Boltzmann constant, T is the absolute temperature, and σ_t is conductivity at any temperature.

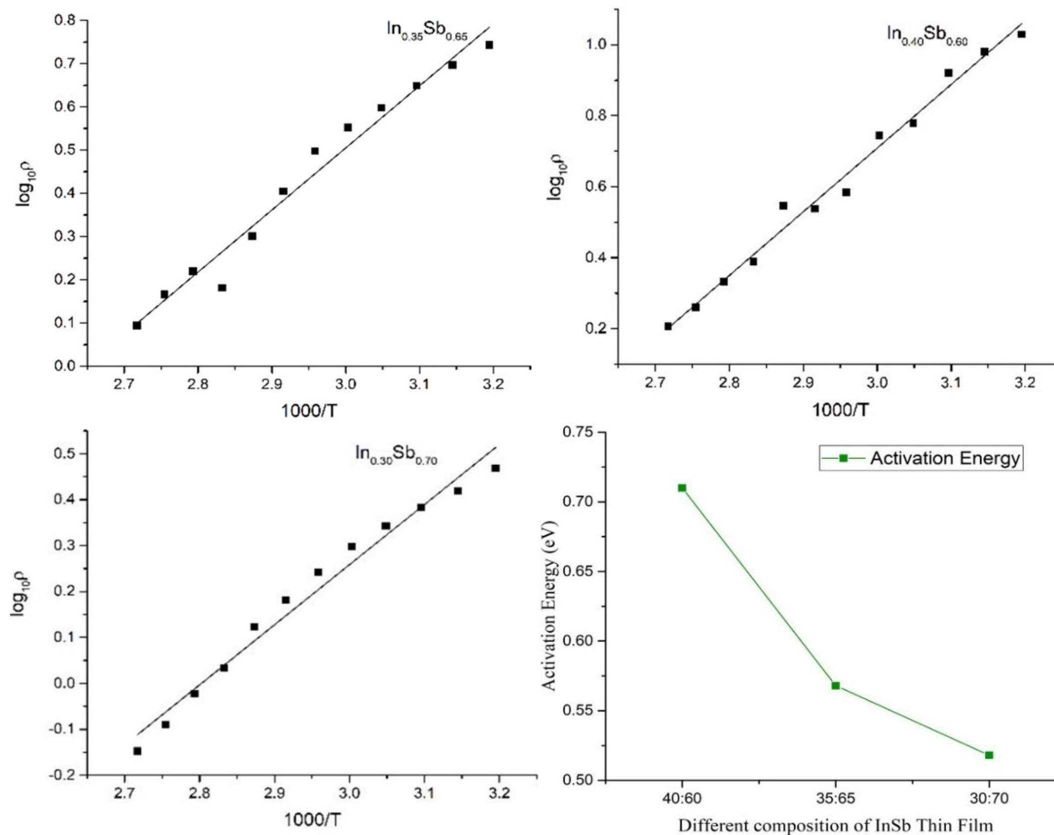

Fig. 8. Variation of Activation energy band gap of different compositions of InSb thin film.

3.7.3. Hall measurement

The Hall effect is studied by inducing a magnetic field perpendicular to the current flow direction in the surface of InSb thin film. Under such conditions, a hall voltage is developed perpendicular to both the current and magnetic field. The developed hall voltage observed by considering the force on a charged carrier in the presence of a magnetic field is shown in the following equation.

$$\vec{F} = q\vec{E} + q\vec{v} \times \vec{B}$$

The total electric field drives the current through the sample in the above expression's first term, while the second term arises from the presence of Lorentz forces on the charged carriers, which tend to deflect charged carriers toward the sample's side. The charge carriers' sign, which identifies the type of semiconductor, depends on the direction of deflection. The following formula is used to calculate the hall coefficient, carrier concentration, and mobility and is shown in Table 3.

$$R_H = \frac{V_H \times d}{I_x \times B_z} \quad (8)$$

$$n = \frac{1}{R_H \times q} \quad (9)$$

$$\mu = \frac{R_H}{\rho} \quad (10)$$

where d is the thickness of the thin film, I_x is the applied current in the x-direction, B_z is the applied magnetic field in the Z-direction, and ρ is the thin film's resistivity. R_H stands for the Hall

coefficient, n is carrier concentration and μ is the mobility, V_H is Hall voltage. The electrical parameter such as sheet resistance, sheet concentration, and Hall coefficient decreases with increasing antimony in the composition tabulated in Table 3. The hall coefficient reveals the fabricated thin films are p-type. The electrical resistivity decreases with the increase of antimony (Sb) in the samples. The carrier concentration gets increases due to electrical resistivity decreases. The activation energy of the thin films is tuned with increasing antimony in composition and can be used in junction diode and junction transistor applications[18].

Table 3. Electrical properties of InSb thin.

Sample	Resistivity (Ohm-cm)	Sheet Resistance (Ω/sq)	Conductivity (S/cm)	Bulk concentration (Cm^{-3})	Sheet Concentration (Cm^{-2})	R_H (Cm^3/C)	Mobility (Cm^2/V-s)	Activation Energy (eV)
$In_{.40}Sb_{.60}$	3.63	12.1E +04	2.75E-01	8.81E+17	2.64E+13	7.09	1.953	0.710
$In_{.35}Sb_{.65}$	1.88	6.27E+04	5.32E-01	19.1E+17	5.72E+13	3.28	1.744	0.568
$In_{.30}Sb_{.70}$	0.997	3.32E+04	1.00E+00	46.3E+17	13.9E+13	1.35	1.354	0.518

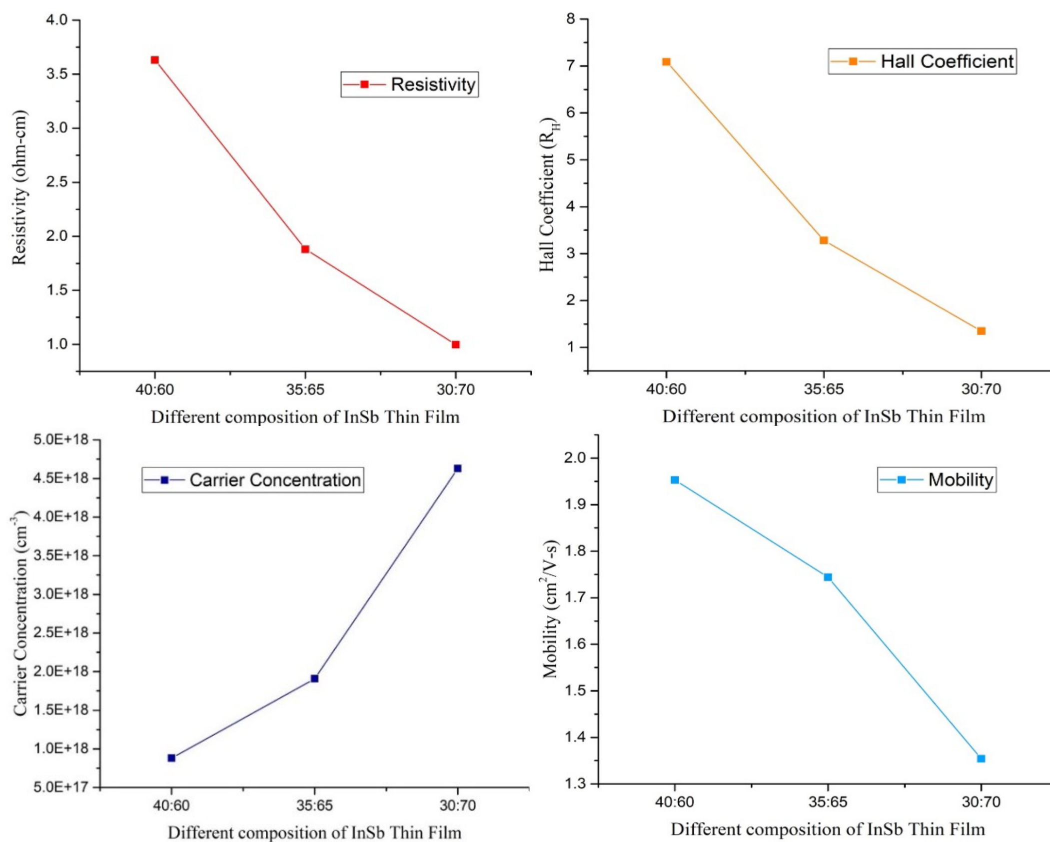

Fig. 9. Variation of Electrical Resistivity, Hall coefficient, Carrier Concentration, and Mobility with the different composition InSb thin film.

3.8. Optical Properties

The optical band gap of InSb thin films measured by ultraviolet-visible (UV-Vis) spectroscopy is a commonly used technique to determine the optoelectronic properties of the films. The absorption spectrum was recorded for analysis of the optical band gap of indium antimonide (InSb) thin films utilizing UV-Vis spectroscopy. In the absorption spectrum of an InSb thin film, a

sharp edge is observed at a specific wavelength, which corresponds to the optical band gap energy of the synthesized material. The optical band gap energy can be calculated from the absorption edge using the equation:

$$\alpha h\nu = A(h\nu - E_g)^n \tag{11}$$

where $h\nu$is the photon energy, $\alpha$is the absorption coefficient, E_g is the optical band gap of InSb thin films, A is the absorption constant, n= $\frac{1}{2}$ for direct band gap materials, n= 2 for indirect band gap materials.

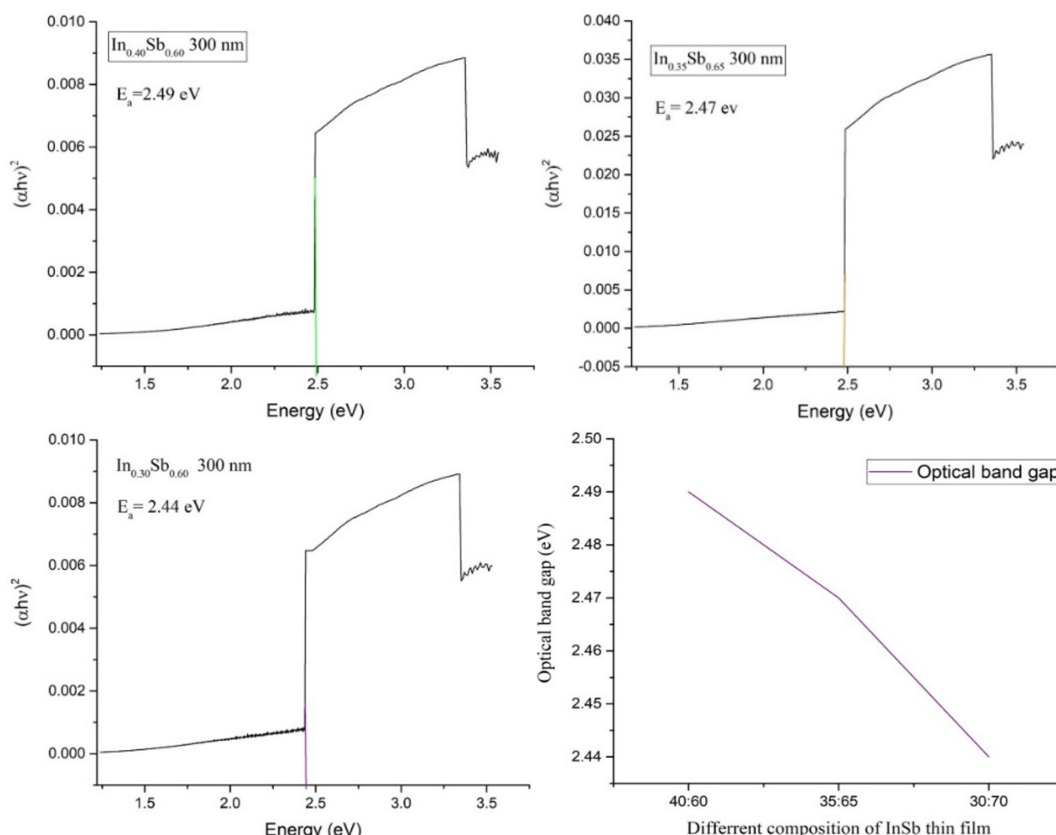

Fig. 10. Variation of the optical band gap of different compositions of InSb thin film.

It should be noted that the optical band gap is influenced by the presence of defects, impurities, and strain present in the films. However, the presence of point defects in the film can cause a shift in the position of the absorption edge, leading to an incorrect measurement of the optical band gap. Hence, it is important to prepare high-quality thin films to obtain accurate results from optical band gap measurements. The optical band gap of $In_{0.40}Sb_{0.60}$, $In_{0.35}Sb_{0.65}$, and $In_{0.30}Sb_{0.70}$thin films was observed and found to be 2.49 eV,2.47 eV, and 2.44 eV respectively. The optical band gap of the film decreases due to a slight increment of the grain size tabulated in Table 2.

3.5. Calculation of critical thickness and lattice-mismatched parameters for Homojunction device

In homojunction $\mathbf{a_S}$ is the lattice parameter of the substrate and $\mathbf{a_L}$ is the lattice parameter of the growing material. In the present study, we take our p-type InSb thin film as a substrate. And other authors as n-type InSb thin film.

The relation between the mismatch parameter (ε), Substrate lattice (a_s), and growing layer lattice (a_L) is given below

$$\varepsilon = \left|\frac{a_S - a_L}{a_S}\right| \tag{12}$$

The critical thickness ($\mathbf{d_C}$) is calculated using the formula

$$d_C = \frac{a_S}{2\varepsilon} \tag{13}$$

In present study p type InSb thin film compare with other author's n type InSb thin film and calculate Lattice mismatch (**ε**)and critical thickness ($\mathbf{d_C}$) which found to 3% and 97 nm, which shown in table 4. The less mismatch of lattice can reduce the nonradiative transition in the optoelectronic device.

Table 4. Lattice mismatch and critical thickness.

S.NO.	Substrate lattice ($\mathbf{a_S}$) P-type InSb nm	Growing layer lattice ($\mathbf{a_L}$)nm	Mismatch Parameter (**ε**)	Critical thickness ($\mathbf{d_C}$) nm	Reference
1	6.7074	6.4840	0.0344	97.49	[2]
2	6.7074	6.4740	0.0348	96.37	[15]

4. Conclusion

Non-stoichiometric InSb compound (cation vacancy) as starting materials of polycrystalline nature with zincblende crystal structure with (111) and (220) plane of orientation has been prepared using molybdenum boat in vacuum for deposition of p-type InSb thin films. The p-type InSb thin films have been deposited on a glass substrate at room temperature of 300 nm thickness by thermal evaporation technique with the use of starting materials. These deposited films are polycrystalline and have a zinc blend structure. Field effect Scanning electron microscopic study confirmed the smooth surface of films and growth of grains is uniform and homogeneous. The Hall measurement indicates that the films were p-type, having a carrier concentration $(0.435 - 1.590)10^{18}$ cm^{-3} and mobility (3.29 – 6.62) cm^2/V-s for the film thickness of 300 nm. The activation energy (E_a) was measured by four probe method and found between 0.710 eV,0.568 eV, and 0.518 eV respectively. The optical band varies by 2.49 eV,2.47 eV, and 2.44 eV respectively.

References

[1] K. E. Hnida, S. Babler, J.Mech, K.Szacilowski, R. P. Socha, M.Gajewska, K. Nielsch, M. Przybylski, G. D. Sulka, J Mater Chem C Mater, vol. 4(2016), no. 6, pp. 1345-1350; https://doi.org/10.1039/C5TC03656A

[2] R. K. Mangal, Y. K. Vijay, Bull. Mater. Sci., Vol. 30(2007), No. 2, pp. 117-121; https://doi.org/10.1007/s12034-007-0021-x

[3] J. Heremans, D. L. Partin, C. M. Thrush, L. Green, Semicond. Sci. Technol. 8 (1993) S424-S430; https://doi.org/10.1088/0268-1242/8/1S/093

[4] M. K. Carpenter, M. W. Verbrugge 1994.

[5] N. K. Udayashankar, H. L. Bhat,Bull. Mater. Sci., Vol. 24(2001), No. 5, October 2001, pp. 445-453; https://doi.org/10.1007/BF02706714

[6] F. W. Wise, Acc Chem Res, vol. 33(2000) no. 11, pp. 773-780; https://doi.org/10.1021/ar970220q

[7] A. D. Yoffe, Adv Phys, vol. 42(1993), no. 2, pp. 173-262;
https://doi.org/10.1080/00018739300101484

[8] M. A. Taher and O. Nittono, Daffodil International University Journal of Science and Technology, Volume 1(2006), Issue 1.

[9] D. K. Gaskill, G. T. Stauf, N. Bottka, Appl Phys Lett, vol. 58(1991), no. 17, pp. 1905-1907;
https://doi.org/10.1063/1.105069

[10] T. Zhang et al, Appl Phys Lett, vol. 84(2004), no. 22, pp. 4463-4465;
https://doi.org/10.1063/1.1748850

[11] S. R. Vishwakarma, A. Kumar, R. S. N Tripathi, S. Das,Indian Journal of Pure and Applied Physics, Vol.51(2013) pp 260-266

[12] S. Boolchandani, S. Srivastava, Y. K. Vijay, J Nanotechnol, vol. 2018(2018);
https://doi.org/10.1155/2018/9380573

[13] R. R. Awasthi, K. Asokan, B. Das, Int J Appl Ceram Technol, vol. 17(2020), no. 3, pp. 1410-1421; https://doi.org/10.1111/ijac.13446

[14] R. R. Awasthi, B. Das, Optik (Stuttg), vol. 194 (2019);
https://doi.org/10.1016/j.ijleo.2019.162973

[15] S. R. Vishwakarma, A. K. Verma, S. N. Tripathi, S. Das, Rahul,Indian Journal of Pure and Applied Physics, Vol.50(2012) pp 339-346.

[16] M. Singh, Y. K. Vijay, Indian Journal of Pure and Applied Physics, Vol.43(2005) pp 383-385.

[17] M. Singh, Y. K. Vijay, Indian Journal of Pure and Applied Physics, Vol. 42(2004) pp 610-614.

[18] V. Senthilkumar, S. Venkatachalam, C. Viswanathan, S. Gopal, S. K. Narayandass, D. Mangalaraj, K. C. Wilson, K. P. Vijayakumar, Crystal Research and Technology, vol. 40(2005), no. 6, pp. 573-578; https://doi.org/10.1002/crat.200410385